ELSEVIER

Contents lists available at ScienceDirect

Sensors and Actuators: A. Physical

journal homepage: www.journals.elsevier.com/sensors-and-actuators-a-physical





Opto-thermoplasmonic pneumatic pistons actuator

Hongbiao Wang^a, Jinliang Xu^{a,b}, Yuqian Zhang^a, Xin Yan^{a,*}, Guohua Liu^{a,b}

- a Beijing Key Laboratory of Multiphase Flow and Heat Transfer for Low Grade Energy Utilization, North China Electric Power University, Beijing 102206, PR China
- b Key Laboratory of Power Station Energy Transfer Conversion and System, North China Electric Power University, Ministry of Education, Beijing 102206, China

ARTICLE INFO

Keywords:
Optofluidics
Pneumatic piston
Nanofluid
Thermoplasmonic
Vapor propulsion

ABSTRACT

Optical manipulation of liquids has extensive applications, ranging from biological research to information technology. However, existing technologies struggle with a fundamental limitation, as the pinning force of the contact line significantly resists liquid motion. In this study, a novel strategy is introduced to govern fluid motion and overcome this barrier. Our approach involves positioning a nanofluid slug within a sealed capillary tube and directing irradiation to one side of the slug. Intensive local vaporization of nanofluid is generated due to the thermo-plasmonic effect of nanoparticles, leading to a considerable driving force and rapid motion of the slug. Based on this principle, the opto-thermoplasmonic pneumatic piston was proposed. The direction of motion is controlled by modulating the laser irradiation direction. Furthermore, the laser beam parameters enable adjustable piston oscillation frequency and speed. To better understand the characteristics of the optothermoplasmonic pneumatic piston, theoretical studies were conducted to analyze the kinetic characteristics of the piston, revealing an expression consistent with the Kelvin-Voigt model. Various factors affecting the performance of the pneumatic pistons were also studied. Based on the experimental results and motion model, we found and explained that the oscillation amplitude presents an exponential relationship with the working frequency $l_a = a(1 - e^{-f_a^{-1}/b})$, where the coefficient a is related to the laser power, slug length, and nanofluid concentration, while the coefficient b is solely dependent on the nanofluid concentration. These optothermoplasmonic pneumatic pistons epitomize a new paradigm for manipulating aqueous mesoscopic systems, thus forging new paths for light-propelled soft motors with precise motion control.

1. Introduction

Actuators are sensors that convert external energy into mechanical motion. Various actuators enhance production efficiency and reduce costs in daily life. They have significant applications in national defense, aerospace, and medical engineering, attracting attention from countries and experts worldwide[1–3]. Their core materials must respond to external stimuli by changing softness, shape, phase, and strength[4,5]. In recent years, light-driven actuators have gained widespread attention, because they enable remote contactless operation and can be used stably in extremely harsh environments[6]. Light-driven actuators are classified into photochemical and photophysical types based on their working principles. Photochemical actuators utilize unique functional groups within the material to undergo reversible photochemical reactions with incident light, imparting different properties to the actuators. For example, chromophoric functional groups like azobenzene can undergo reversible photochemical reactions under visible and ultraviolet light[7,

8]. However, typical photochemical actuators have response times measured in seconds, making them unsuitable for high-frequency applications [9,10]. In contrast, photophysical actuators use physical processes resulting from the interaction between light and material, with response times in the millisecond class. Photothermal actuators are the most common and simple photophysical actuators, which convert light energy into thermal energy, causing deformation or phase changes and triggering actuators operation. A variety of photothermal actuators have been developed. Chen developed an intelligent gripper using a CNT-paper/BOPP combination, which bends significantly under infrared radiation and can lift and move objects twenty times heavier than a single actuator[11]. Vélez-Cordero used laser heating photosensitive materials to make gas in a cavity expanding[12]. The gas driven a liquid column movement to create a light-controlled valve. Meng et al. utilized nanoparticle films to absorb solar energy and convert it into thermal energy, producing a light-driven "motorboat" that moves quickly on the water surface[13].

E-mail address: yanxin@ncepu.edu.cn (X. Yan).

^{*} Corresponding author.

Table 1The comparation of various optical actuators.

Ref.	Actions	Response time	Stimulation	Durability	Highlight
[7]	bend	$< 5~\mu s$	UV light photochemical	> 1000 cycles	Maximum stress is estimated to be 56 MPa
[8]	bend	~10 min	UV light photochemical	> 5 min	Exhibit an expansion and contraction behavior liking a natural muscle
[9]	bend	~30 min	Vis light photochemical	> 4 cycles	Biomimetic curling motions
[11]	bend	10 s	NIR light photothermal	> 100 cycles	The force density is about 51.
[12]	translation movement	1 s	Vis light photothermal	> 40 cycles	The piston is reciprocating motion. Amplitude $<$ 2 mm, $\nu_{max} <$ 0.7 mm/s
[13]	translation movement	~0.3 s	532 nm laser photothermal	-	Moving speed is 34.6 mm/s in water and moving direction can be controlled.
This work	translation movement	~0.2 s	527 nm laser photothermal	> 100 cycles	The energy conversion part and the moving part are combined in the piston which has a quick response and rapid reciprocating movement. Amplitude $<$ 10 mm, $\nu_{max} <$ 1.7 mm/s

The photothermal actuators involve two energy conversion processes: the conversion of light to heat and the conversion of thermal energy into mechanical work. For the first process, the efficiency of light-to-heat conversion is crucial. For commonly used materials, such as metals and semiconductors, about 90 % of incident light is reflected at the air-metal interface, with only 10 % being absorbed and converted into thermal energy[14-16], resulting in very low energy conversion efficiency. In recent years, the use of nanotechnology to construct microstructures on the surfaces of metals and semiconductors has significantly improved light-to-heat conversion efficiency. Nanofluids-mixtures of nanoparticles and base liquids-have seen rapid development over the past decade[17]. Nanofluids possess numerous excellent properties, such as high thermal conductivity, superior optical characteristics, and low viscosity[18]. They can enhance light-to-heat conversion efficiency through plasmonic effects, nearly 100 % absorbing the light and converting it into thermal energy[19]. This enhancement can significantly improve the performance of photothermal actuators.

The application of nanofluids in photothermal actuators is a research branch of optofluidics. Optofluidics is a paradigm for the actuation by using optical forces or light-induced capillary forces[20-22]. The capillary actuation has advantages over the optical force since it doesn't need special optical setups. While the capillary force causing by wettability gradient is too weak to surmount the contact-line pinning, thus limiting the motion in a short distance at low speed. [6,23,24] Recently, the Marangoni force, induced by surface tension gradients, has been used to manipulate particles within fluids [25,26]. However, this method requires a two-phase system to generate a liquid-gas interface, which limits its range of applications and the types of objects it can affect. The nanofluids can be heated to intense boiling under a laser irradiation [27]. The rapid vapor generation, resulting in momentum and pressure variations, would be a promising source of power[28]. The drive force generated by pressure variation is powerful enough to overcome the contact-line pinning.

Herein, we demonstrate an opto-thermoplasmonic pneumatic piston fabricated by loading a liquid slug of gold nanofluid in a sealed capillary glass tube. The device is named for its ability to mimic the reciprocal motions of a piston, performing oscillating movements of the slug via asymmetric thermoplasmonic-induced vapor generation. The collective heating of gold nanoparticles is confined at the vapor/liquid interface, leading to intense heating with a high evaporation rate. The piston can move rapidly, and its oscillation behavior can be easily regulated by adjusting the laser power. A systematic investigation of the oscillating behavior was conducted to study the impact of parameters such as laser power, piston length, and nanofluid concentration. Compared with existing technology (as listed in Table 1), our vapor-enabled device has shorter response time and great motion performance. This piston exhibits a novel capsule structure and fuel-free oscillation, which will be

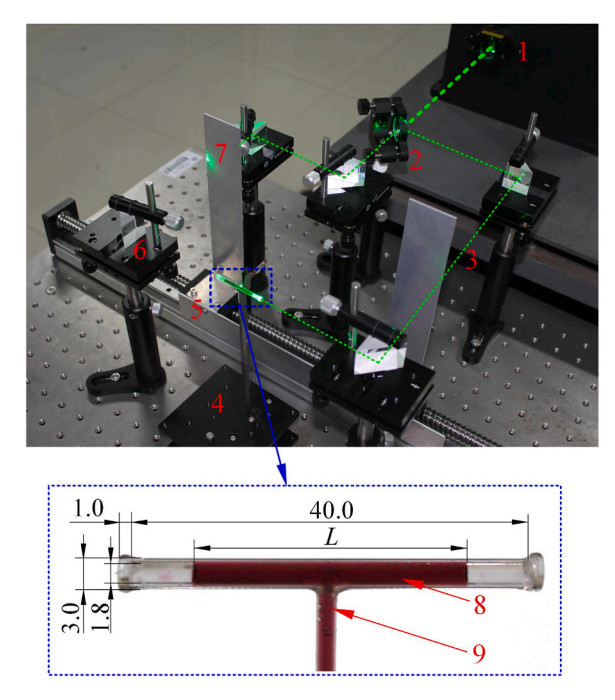


Fig. 1. Experimental setup (1, laser device; 2, beam splitter; 3, laser beam; 4, experimental platform, 5, guide rail; 6, reflective prism; 7, light baffle; 8, gold nanofluid piston; 9, liquid injection tube).

helpful in designing new fluidic machines for cargo transport and biomedical applications.

2. Materials and methods

The actuator was fabricated from PMMA. The entire fabrication process of the piston was as follows: 1) the two ends of a transparent T-shaped tube were sealed with small circular plates; 2) the tube was then vacuumed; 3) a certain amount of the nanofluid was injected into the tube driven by external air pressure; 4) finally, the liquid-injection tube was sealed, with two cavities reserved at both ends (as shown in Fig. S1). The main tube has a length of 4 cm, an inner diameter of 1.8 mm, and a wall thickness of 0.60 mm (Fig. 1). The inner diameter of the actuator was less than the capillary length of the nanofluid (\sim 2.7 mm), ensuring that the liquid piston consistently isolates the cavities at both ends during oscillation. The nanofluids in tube serves as energy conversion part and the executive element, which substantially reduces both the cost and difficulty of making actuators. Depression boiling and vacuum injection were employed to remove non-condensable gases from the

Table 2
Key parameters of the pistons used in this study.

Case	L	c
A1	20 mm	100 ppm
A2	20 mm	200 ppm
A3	20 mm	500 ppm
A4	30 mm	100 ppm
A5	30 mm	500 ppm

Note: L: length of liquid slug; c: concentration of nanofluid

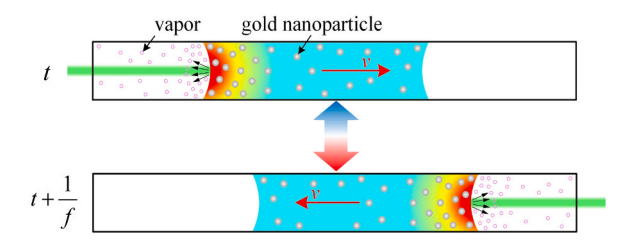


Fig. 2. The working principle of opto-thermoplasmonic pneumatic pistons. The vapor generation at air/liquid interface and differential pressure propels the fluid slug to move forward.

nanofluid. Nanofluid optical properties directly impact actuator performance, especially spectral and photothermal conversion. The concentration of nanofluids influences photothermal efficiency. Table 2 lists key parameters of the five pistons used in this study.

The gold nanofluid is a stable and homogeneous solid-liquid mixture of gold nanoparticles dispersed in water, which exhibits a remarkable proficiency in photothermal conversion. Gold nanofluids were prepared by sodium citrate reduction method[29]. There are gold nanoparticles and sodium citrate, acting as the stabilizer, in gold nanofluids. The detailed characterization of gold nanofluid is shown in Fig. S2. The gold nanoparticles are spherical, and average diameter is 17.13 nm with analyzing 179 nanoparticles (as shown in Fig. S2a, b). Higher concentrations contain more gold nanoparticles. For 100 ppm, about 1.96×10^{12} nanoparticles are involved in one milliliter gold nanofluid. The spectral transmittance of the nanofluid diminishes progressively with increasing nanofluid concentration (shown in Fig. S2c). Notably, at λ = 520 nm, the transmittance reaches its nadir where the plasmonic effect of gold nanoparticle excited. The laser wavelength used in the experiment is 527 nm. As shown in Fig. S2c, the gold nanofluid also exhibits strong absorption of incident light at λ = 527 nm. The absorption length L_a is defined as the distance in the solution required to absorb 90 % of the incident light energy. This parameter reflects the concentration of incident energy and is solely depended on the nanofluid concentration. The L_a decreases as the nanofluid concentration increases, indicating that higher concentrations result in more concentrated laser energy at the liquid-air interface. At a concentration of 500 ppm, the gold nanofluid absorbs 90 % of the light energy within a 1.5 mm liquid film (shown in Fig. S2d).

The experimental setup is depicted in Fig. 1a. The actuator was mounted on a platform capable of precise adjustments to ensure the coaxial alignment of the liquid piston with the light beam. A laser device emitting a beam at 527 nm was used, and the beam was split into two identical beams with a spot size of 1.5 mm using a beam splitter. Reflecting prisms directed the beams to irradiate the liquid piston from both ends. Each light pathway was equipped with a baffle moving at 1 m/s to switch the incident beams on and off, allowing only one side of the laser to pass through the baffle. The operation of the actuator relied on plasmonic heating of the nanofluid, which generated intensive vapor and differential pressure to drive the piston movement (Fig. 2). The motion of the liquid piston was tracked and recorded using a high-speed camera and an infrared camera operating at 100 Hz, both controlled by a synchronizer.

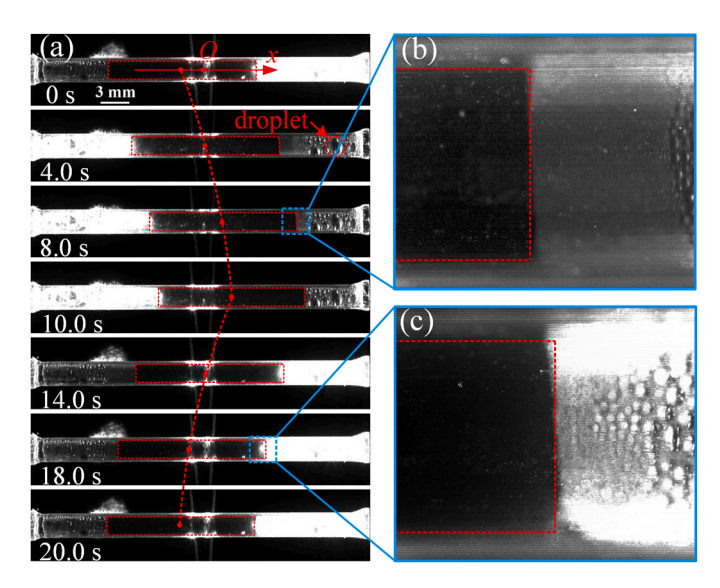


Fig. 3. Images of actuator working (a: the position of liquid-piston moving; b: enlarged right air-liquid interface when laser power off; c: enlarged right air-liquid interface when laser power on; Case A3, P = 1.5 W, f = 0.05 Hz.).

3. Results and discussion

3.1. Actuators characteristics

The complete motion process of actuator A3 over one cycle is illustrated in Fig. 3a. The laser power is set to 1.5 W with an irradiation switching frequency of 0.05 Hz. Initially, the liquid piston is positioned on the left side of the tube, with the incident laser switching from the right side to the left. This causes intensive local vaporization at the left interface of the piston, leading to a significant increase in cavity pressure as vapor gas fills the left cavity, propelling the piston to move right. At 10 seconds, the liquid piston reaches the far-right end, after which the laser switches incident direction, causing the piston to change its moving orientation and return to its initial position at 20 seconds, completing one motion cycle. The red dashed line in Fig. 3a represents the trajectory of the liquid piston within the actuator. The trajectory in half a cycle exhibits nonlinear properties over time, with the piston's velocity gradually decreasing. Figs. 3b and 3c provide enlarged images near the heating interface with and without light irradiation, respectively. Numerous small droplets accumulated on the tube wall by vapor condensation verify that laser irradiation results in nanofluid evaporation, and the vapor propels the liquid piston. During the piston's motion, droplets within the travel range are periodically merged and absorbed by the piston, ensuring long-term stable operation of the actuator.

As shown in Fig. 3a, the liquid piston positioned on the left side of the actuator is set as the initial state. The origin of coordinates is located at the midpoint of the actuator, with rightward motion of the liquid piston considered positive. The motion curve of the actuator's liquid piston was obtained using high-speed camera images. Fig. 4 shows the motion curves of actuator A3 under different laser switching frequencies. The laser heating power was set at 1.5 W. The liquid piston oscillated from one side to the other in the actuator, following the laser switching direction. The oscillatory motion frequencies ranged from 0.05 Hz to 3.6 Hz. The motion of the pistons in the actuator is presented in Movie S1 of the Supplementary Material. In Fig. 4a, the black curve represents the motion of the piston within the actuator, exhibiting a sawtooth waveform with good periodicity, repeatability, and stability. The blue curves represent the absolute value of the piston's instantaneous velocity, calculated from the motion curve (black curve). The liquid piston reaches its maximum velocity (2.6 mm/s) when changing direction, then gradually decreases to \sim 0.1 mm/s as it moves. Both the movement and velocity curves of the piston exhibit exponential decay

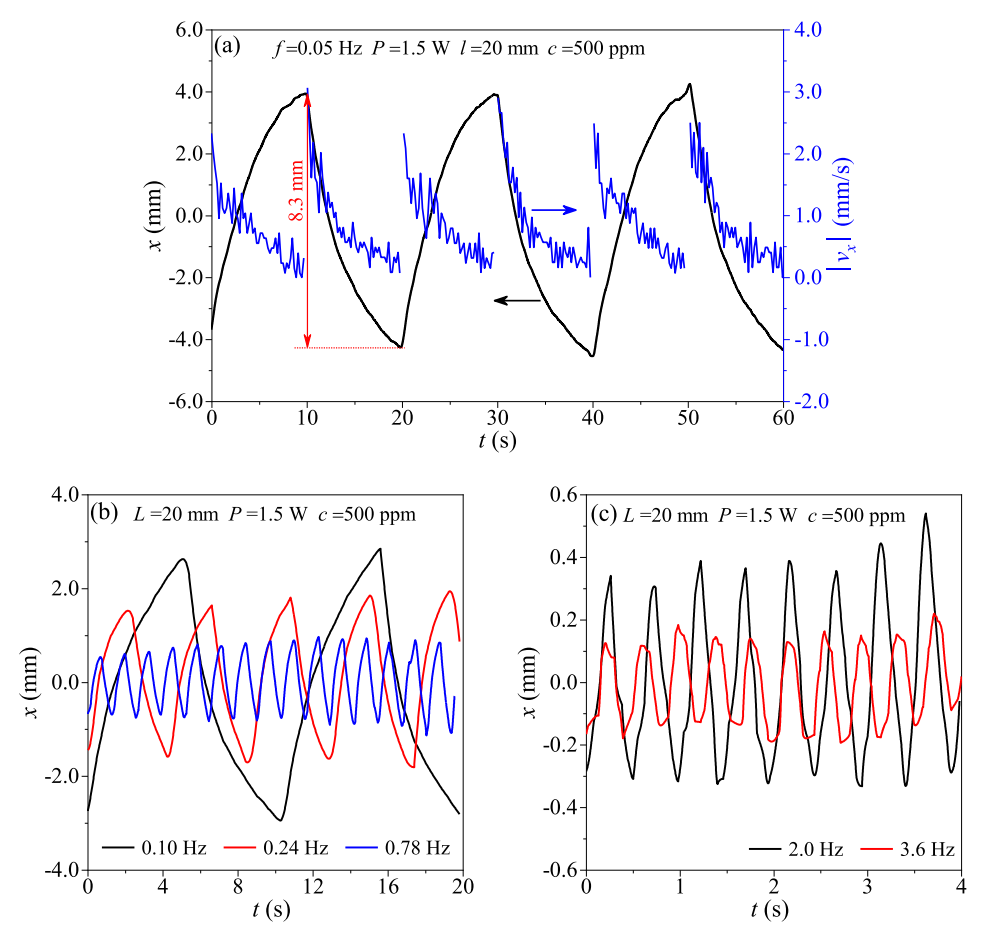


Fig. 4. Displacement of the liquid piston versus time for the A3 actuator at different frequencies f. The laser power in all cases is 1.5 W.

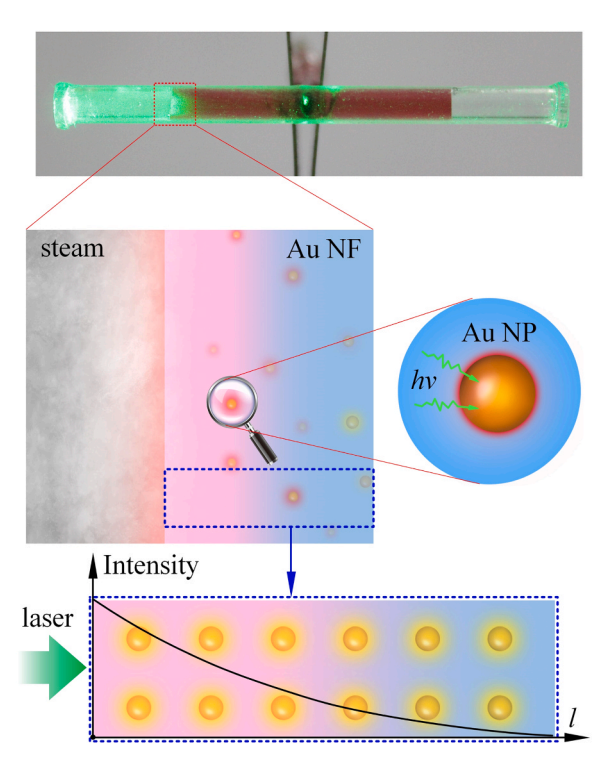


Fig. 5. The scheme diagram of heat generation and localization (the physical model of photo-thermal conversion).

characteristics. With increasing laser switching frequency, the liquid piston continued to move regularly from one side to the other. However, the motion amplitudes decreased from 8.3 mm to 0.35 mm. The maximum amplitude of the liquid piston in Fig. 4 reaches \sim 8 mm, significantly exceeding the motion amplitudes (\sim 1 mm) of optically driven actuators reported in the literature [12,30]. The amplitude and velocity of the liquid piston motion in the actuator indicate that the influence of the contact line pinning force on the liquid piston is minimal and can be neglected. The actuators in this study exhibit a better signal-to-noise ratio. In future work, the process of energy conversion and the influence of various factors will be investigated to study the operational characteristics of the actuators.

Supplementary material related to this article can be found online at doi:10.1016/j.sna.2025.116515.

The nanofluid piston is a crucial component for energy conversion and movement in the proposed actuator. Its photothermal capability is closely linked to the actuator's performance. The liquid piston is required to exhibit high optical absorption and excellent photothermal conversion ability to generate vapor. In this study, gold nanofluid is selected to create the liquid piston. The gold nanoparticles in the nanofluid interact with the incident laser, where the free electrons inside the nanoparticles oscillate in resonance with the laser, a phenomenon called the plasmonic effect. This enhances optical absorption and facilitates the conversion of optical energy into thermal energy [27]. The nanoparticles' temperature rapidly rises. Heat is then dissipated into the water through thermal conduction, leading to temperature increases and vapor generation, as depicted in Fig. 5. Nanofluid vaporization increases the cavity pressure, inducing a pressure difference between the cavities on both sides of the liquid piston, propelling the piston's movement. The incident laser undergoes exponential decay within the

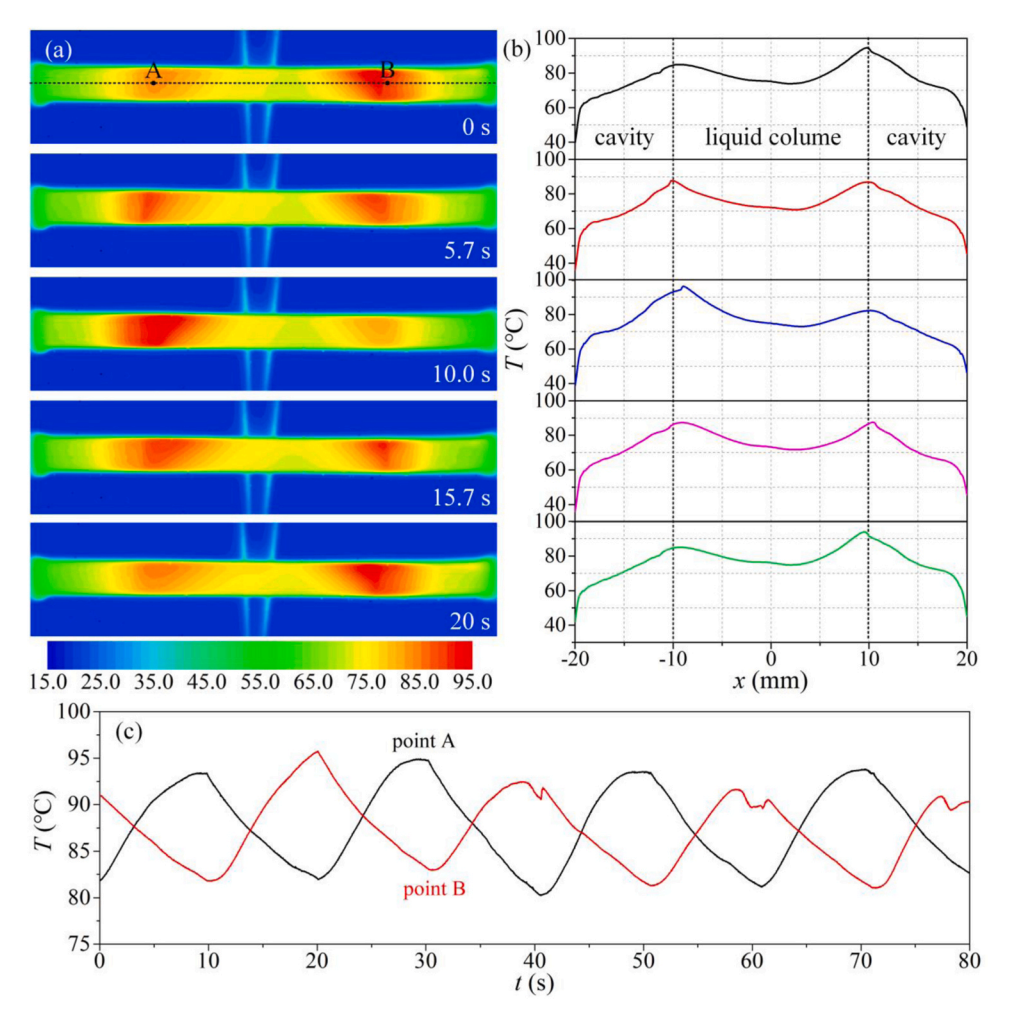


Fig. 6. The spatial distribution of actuator temperature (a: temperature map of actuator for P = 1.0 W, c = 500 ppm, L = 20 mm and f = 0.05 Hz; b: temperature at actuator axes showing bimodal distribution; c: dynamic temperature at air-liquid interfaces of point A and B).

gold nanofluid, with the majority of laser energy concentrated near the nanofluid slug interface. Furthermore, as nanofluid concentration increases, energy concentration becomes more pronounced, facilitating rapid vaporization at the gas-liquid interface and enhancing energy utilization efficiency. These results are supported by Mie's scattering theory and the Radiative Transfer Equation (as shown in the Supplementary Material).

The energy conversion and thermal inertia of the actuator are demonstrated through the temporal and spatial variation of the temperature during its operation. Fig. 6a shows the temperature field variation of the actuator over one cycle at a frequency of 0.05 Hz (dynamic temperature variation can be seen in Movie S2 of the Supplementary Material). The temperature distribution within the liquid piston follows a "high-low-high" pattern, with two hot spots located near the piston's vapor/liquid interfaces. The temperature in the middle of the piston remains nearly constant. The temperatures of these hot spots alternate, rising and falling with time, consistent with the switching period of the laser beam, indicating minimal thermal inertia in the actuator. The upper temperature of the liquid piston is higher than the lower part (as shown in Fig. 6a), attributed to the upward movement of high-temperature fluid due to buoyancy.

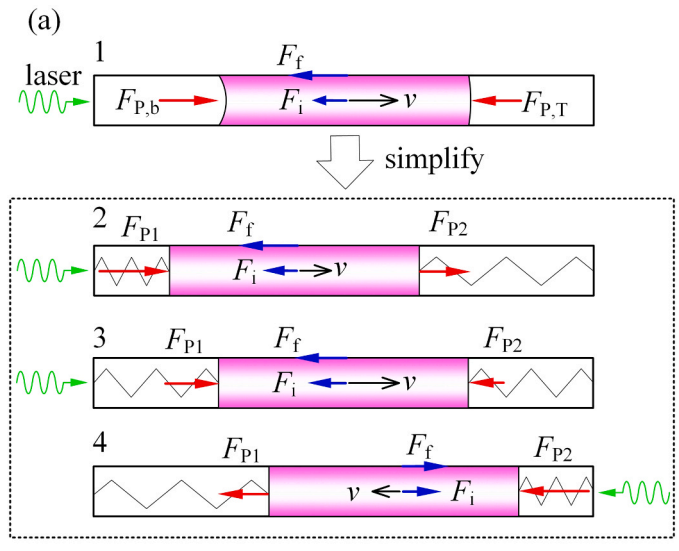
Supplementary material related to this article can be found online at doi:10.1016/j.sna.2025.116515.

Fig. 6b shows the temperature variation along the central axis of the actuator, corresponding to the dashed line in Fig. 6a. A bimodal pattern is observed, with the highest temperatures occurring at both ends of the liquid piston. The temperature decreases rapidly away from the

interface. The curves on both sides of the black dashed line represent the temperatures of the cavities, while the central part represents the temperature of the liquid piston. The higher temperatures at the piston ends compared to the middle are due to the concentration of laser energy, facilitating rapid vapor generation. Heat in the middle of the liquid piston is primarily conducted from the ends. During actuator operation, heat conduction in the middle of the piston balances out dissipation, maintaining a constant temperature there. Fig. 6c shows the temperature variations over time at the left and right ends of the liquid piston (points A and B in Fig. 6a). A periodic rise and fall in temperature, in sync with the laser beam switching, is observed. The temperature rise indicates optical energy absorption by the nanofluid, converting energy into heat, while the temperature decrease signifies rapid heat dissipation from the shell. The consistency between temperature variation and piston movement demonstrates that the motion is propelled by vapor generation at the ends of the liquid piston. The rapid photothermal conversion and dissipation of the piston contribute to the actuator's minimal thermal inertia and quick response capability.

3.2. Motion model of actuators

The dynamic performance of piston can be further understood by force analysis. Fig. 7a shows a diagram of force analysis of the liquid piston, and the main forces involving the working process include the pressure forces $F_{P,b}$, $F_{P,T}$, the friction force F_f and the inertia force F_i . The force balance equation is as follows:



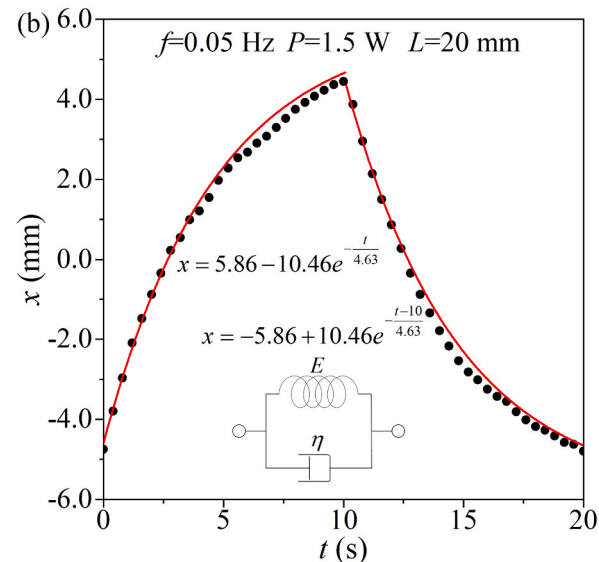


Fig. 7. Physical model for actuator and curves fitting for liquid-piston movement data. The inset in Fig. b is a kelvin module unit, which has elastic (E) and viscous (η) components.

$$F_i + F_f = F_{P,b} - F_{P,T} = (p_1 - p_2)S$$
 (1)

where F_i =ma. We consider the nanofluid piston as incompressible fluid with no-slip boundary conditions. The movement of the liquid piston in actuator is a laminar flow and a quasi-static process. Thus, the flow field of liquid piston follows the Hagen-Poiseuille laminar flow, and the friction force between the piston and tube wall can be described as: [31]

$$F_{\rm f} = 8\pi L \mu \overline{u} \tag{2}$$

where μ is the liquid dynamic viscosity, \overline{u} is the average velocity of fluid, and L is the length of liquid piston. In addition, the inertial force F_i can be ignored due to a small mass of liquid piston. Then Eq. (1) can be written as

$$8\pi L\mu \overline{u} = (p_1 - p_2)S \tag{3}$$

Since $\overline{u} = dx/dt$, we get

$$8\pi L\mu \frac{dx}{dt} = (p_1 - p_2)S \tag{4}$$

Solving the differential Eq. (4) yields an analytical solution for the liquid piston movement. The pressure difference on the right side is the

key important to solve the equation.

The pressure driving the liquid piston movement comes from the vapor pressure and the volume change of the cavity. The piston in actuator over a cycle is controlled by spring force, friction force and a driven force, as shown in Fig. 7a. Assuming the water vapor in the cavity behaves as an ideal gas, the following equation is derived based on the ideal gas equation $pV=nR_gT$.

$$\left(p_1 - p_2\right) S = R_g T n \left(\frac{1}{0.5L_0 - l_0 + x} - \frac{1}{0.5L_0 + l_0 - x}\right)$$
 (5)

Where R_g is the gas constant; n represents the number of water molecules that vaporize or condense over a cycle; T is the temperature of vapor; L_0 is the total length of the cavities on both sides. Substituting Eq. (5) into (4) yields

$$8\pi L\mu \frac{dx}{dt} = R_g Tn \left(\frac{1}{0.5L_0 - l_0 + x} - \frac{1}{0.5L_0 + l_0 - x} \right)$$
 (6)

Solving the equation, we get

$$-\frac{L_0^2}{8}\ln(l_0 - x) + \frac{1}{4}(l_0 - x)^2 = \frac{R_g Tn}{8\pi Lu}t + C_1$$
 (7)

To further simplify, the second item of above equation is neglected, yielding

$$x \approx l_0 + Ce^{-\frac{P_g}{8\pi L\mu}t} \tag{8}$$

Where l_0 physically signifies the position where the piston velocity decreases to zero; $P_g = 8R_gTn/L_0^2$, defined as the stiffness coefficient of the vapor within the cavity. According to the definition formula, the stiffness coefficient is related to the vapor quantity, temperature, and cavity volume. The vapor quantity inside the cavity is a function of laser power P and nanofluid concentration c; the cavity volume is related to the piston length L (for actuators with the same actuator length) and the liquid piston position x; the average vapor temperature remains essentially unchanged during laser irradiation, as shown in Fig. 6. Thus, the stiffness coefficient P_g is defined as a function of the piston length L, laser power P, and nanofluid concentration c, and written as $P_g = g(L, P, c)$. Substituting the known parameters into Eq. (8) and fitting with the motion curve, the values of l_0 , P_g and C thus can be determined.

The fitting curves using Eq. (8) with experimental data are compared in Fig. 7b. The black dots represent the experimental data of the liquid piston motion, while the red curve represents the fitting results using Eq. (8). The red curves fit the experimental data quite well. Eq. (8) conforms to the Kelvin model in viscoelastic theory, implying that the oscillatory movement of the liquid piston can be decomposed into elastic and viscous components[32] (as shown in the inset of Fig. 7b). The frictional force F_f between the piston and the tube wall acts as the viscous element η , while the vapor pressure p_2 -S in the compressed side cavity acts as the elastic element E, and the vapor pressure p_1 -S in the irradiated side cavity provides the driving force for piston motion.

3.3. The impact of different parameters

Fig. 8 shows the motion curves and the relationship between oscillation amplitude l_a and laser switching frequency f_a for different actuators (as listed in Table 2) under various conditions. Laser power P, liquid piston length L, and nanofluid concentration c significantly impact the actuator's working characteristics. Fig. 8a illustrates the movement curves of the piston in actuator A3 under laser power of 1 W and 1.5 W, respectively. Due to the excellent photothermal vaporization characteristics of the nanofluid, the thermal inertia of the liquid piston is very low. The actuator quickly responds to changes in the laser irradiation position, exhibiting broad adaptability to laser powers. The travel distance of the liquid piston increases with heating power. This is the result of two opposing factors. Firstly, increasing the laser power

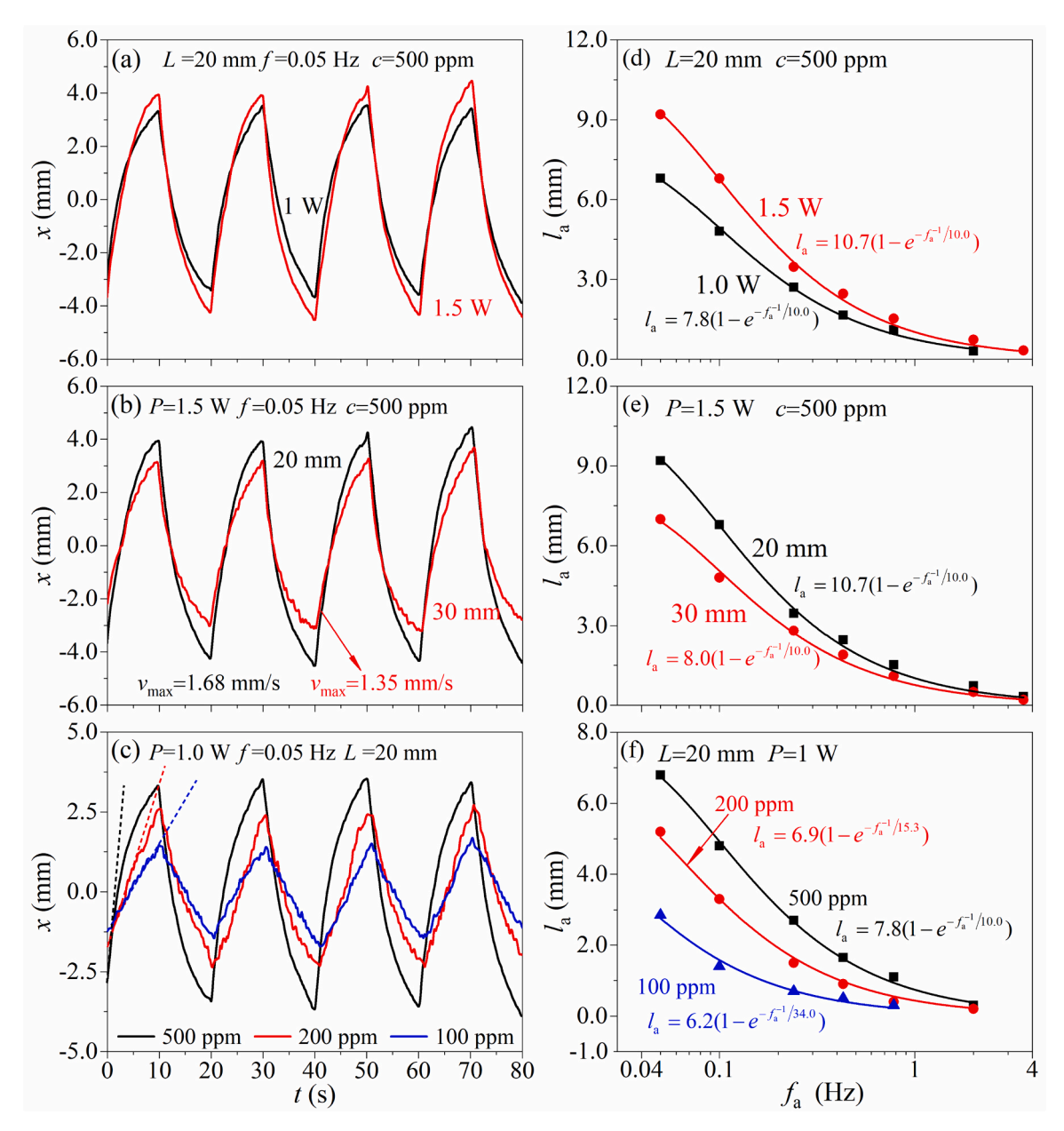


Fig. 8. Effect of *P*, *L* and *c* on displacement and amplitude of air-liquid interface (a, b and c: displacement of air-liquid interface versus time for different cases; d, e and f: and amplitude of air-liquid interface versus frequency for different cases).

enhances the vaporization rate of the nanofluid, increasing the external force driving the piston movement and correspondingly enlarging the piston oscillation amplitude. Secondly, increasing the laser power increases the vapor quantity in the cavity, which will be compressed in the next half cycle, impeding the piston's movement in the next half cycle. These two opposing mechanisms result in the piston oscillation amplitude nonlinearly increasing with laser power.

Increasing the piston length L decreases the motion amplitude (see Fig. 8b). On one hand, a longer piston increases motion resistance and weakens the influence of the driving force. On the other hand, as the piston length increases, the volume of the cavities in the actuator decreases. Actuators with longer pistons have larger vapor pressure in the cavities for the same working duration. This increases the elastic modulus of the actuator, resulting in smaller displacements of the piston under the same driving force. As shown in Fig. 8b, the piston with a length of 20 mm has a larger $\nu_{\rm max}$ than the one with a length of 30 mm. Friction between the piston and the tube wall hinders rapid changes in piston speed[32], slowing down the actuator's response rate.

Additionally, frictional force dissipates the kinetic energy of the piston, affecting the efficiency of energy conversion.

Compared to laser power P and liquid piston length L, the nanofluid concentration c has the greatest impact on the actuator's working characteristics (as shown in Fig. 8c). Both the oscillation amplitude l_a and the maximum velocity v_{max} of the piston increase with rising nanofluid concentration. It can be observed that the motion curves of the piston with different nanofluid concentrations are triangular waveforms, but the degree of nonlinearity of the curves increases with increasing nanofluid concentration. The dashed lines in Fig. 8c represent the tangent line of the curves at the initial moment. The motion curve with c=100 ppm coincides with the dashed line. As the nanofluid concentration increases, the deviation of the curves from the dashed line increases. These changes are mainly related to the absorption length L_a for nanofluids with different concentrations. As the nanofluid concentration increases, the laser energy is absorbed by a thin liquid layer after entering the liquid piston. This thin liquid layer converts into vapor, causing the vapor pressure in the cavity with laser irradiation to rise

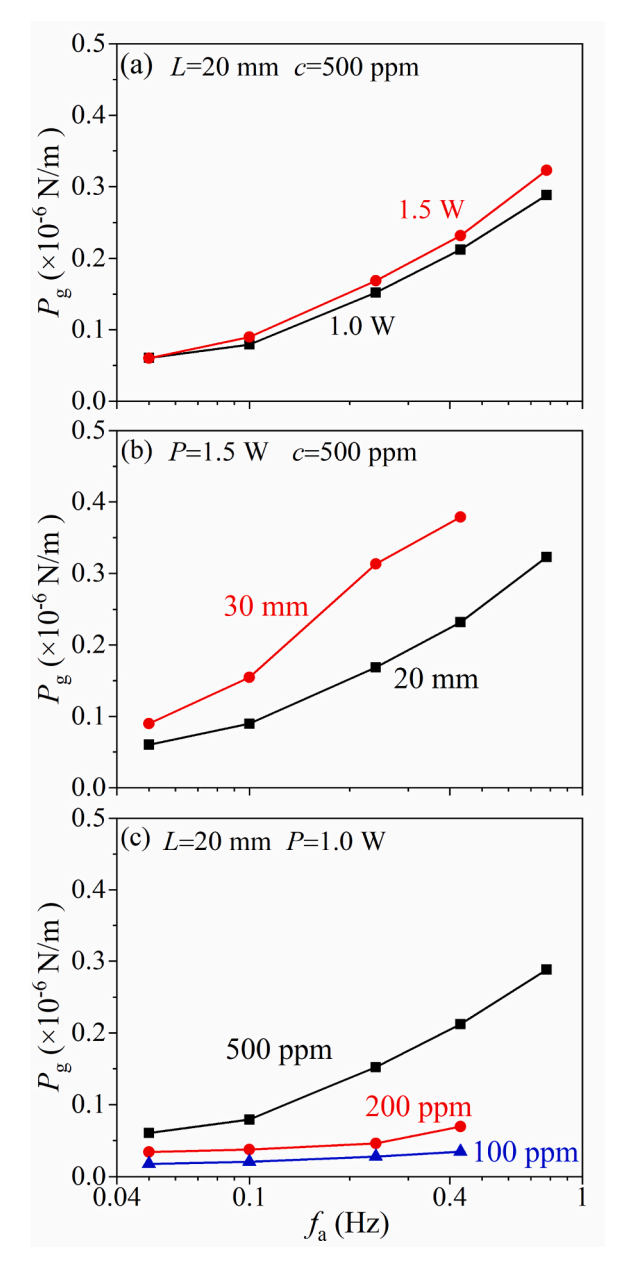


Fig. 9. Effect of P, L and c on stiffness factor P_g .

rapidly, resulting in large maximum velocity ν_{max} and oscillation amplitude l_a in a short time. However, as the piston moves, its momentum is consumed by frictional forces, decreasing the velocity and leading to nonlinear characteristics. For a liquid piston with low nanofluid concentration, most of the laser energy is converted into sensible heat. The vapor generation rate is low, causing the force driving piston motion to equal the frictional force between the piston and the tube wall. The motion of the piston tends toward uniform rectilinear motion, as represented by the blue curve in Fig. 8c.

Fig. 8d-f are the relationships between the oscillation amplitude l_a and the frequency f_a under different conditions. It is observed that both the data obey an exponential decay relationship of $l_a = a(1 - e^{-f_a^{-1}/b})$. Note that f_a^{-1} represents the actuator working period T_a . Thus, the relationship can also be rewritten as $l_a = a(1 - e^{-T_a/b})$. The values of a and b are obtained from curve fitting. The coefficient a reflects the amplitude magnitude of the piston, while the coefficient b reflects the variation trend of the amplitude against frequency (period). It is shown that the coefficient a is related to laser power a, liquid piston length a.

and nanofluid concentration c. However, coefficient b is only controlled by nanofluid concentration c. It's easy to understand that increasing the driving force (i.e., increasing laser power P and nanofluid concentration c) and decreasing the motion resistance (i.e., reducing the piston length L) can enlarge the oscillation amplitude. The data in Fig. 8d-f also validate this conclusion. Latter, the reasons why coefficient b is only related to nanofluid concentration will be analyzed.

According to Eq. (8), the oscillation amplitude can be expressed as:

$$l_{a} = x \left(\frac{T_{a}}{2}\right) - x(0) = -C \left(1 - e^{-\frac{P_{g}}{16\pi L\mu}T_{a}}\right)$$
 (8)

Comparing Eq. (8) with $l_a=a(1-e^{-T_a/b})$, the a=-C and $b=16\pi L\mu/P_g$ can be obtained. Thus, the coefficient C in Eq. (8) represents a constant characterizing the amplitude of piston, while the coefficient b is related to the viscous friction and stiffness coefficients of the actuator. The expression of the stiffness coefficient P_g is not yet fully clear. According to the definition of the stiffness coefficient $P_g=g(L,P,c)$, the following section will discuss the effects of the laser power P, liquid piston length L, and nanofluid concentration c on the stiffness coefficient P_g .

Fig. 9 illustrates the relationship between the stiffness coefficient P_g and various factors. (1) As shown in Fig. 9a, the differences between the two curves are small, indicating that the laser power P has little effect on the stiffness coefficient. Analyzing the dynamics of the piston, P_g primarily reflects the compression capability of the vapor in the compressed side cavity, which is not heated by the laser during piston movement. Thus, the stiffness coefficient is minimally affected by laser power. (2) With increasing piston length L, the stiffness coefficient increases (as shown in Fig. 9b). An increase in piston length implies a decrease in cavity volume, allowing a small amount of vapor to generate significant pressure, hindering the movement of the piston. Therefore, the longer piston has a smaller oscillation amplitude $l_{\rm a}$ and maximum velocity v_{max} , as depicted in Fig. 8b and e. It is noted that, under different frequencies, the P_g for a 30 mm liquid piston is approximately 1.5 times that for a 20 mm liquid piston. Thus, for the constant actuator length, P_{g} is approximately proportional to the piston length. (3) A larger nanofluid concentration c results in a greater stiffness coefficient P_g . With an increase in nanofluid concentration, the laser power is absorbed over a limited distance, resulting in a higher temperature there. Switching to the next half-cycle, the piston remains at a high temperature, increasing the saturation vapor pressure in the compressed side cavity and thus enlarging the stiffness coefficient.

Overall, the stiffness coefficient $P_{\rm g}$ is primarily influenced by the liquid piston length L and nanofluid concentration c. Considering that the viscous friction force and stiffness coefficient are both proportional to the liquid column length L, it can be deduced from Eq. (8) that coefficient b is only influenced by the nanofluid concentration c. Therefore, the nanofluid concentration is the most important factor influencing actuator performance. A high-concentration nanofluid can concentrate the light energy in a microscale domain, which not only reduces the absorption length but also increases the oscillating amplitude as well as the response rate at high frequency.

3.4. Comments and perspective

In opto-thermoplasmonic pneumatic pistons actuator, the light energy transforms into heat, which is then converted into the kinetic energy of liquid column movement. Photothermal conversion efficiency mainly depends on the nanofluid's optical properties, concentration, and laser wavelength. Photothermal conversion is optimized when the incident wavelength aligns with the nanofluid's absorption peak. In this study, the superior optical properties of gold nanofluids enable 100 % photothermal conversion efficiency. The conversion efficiency of thermal energy to kinetic energy is primarily influenced by the

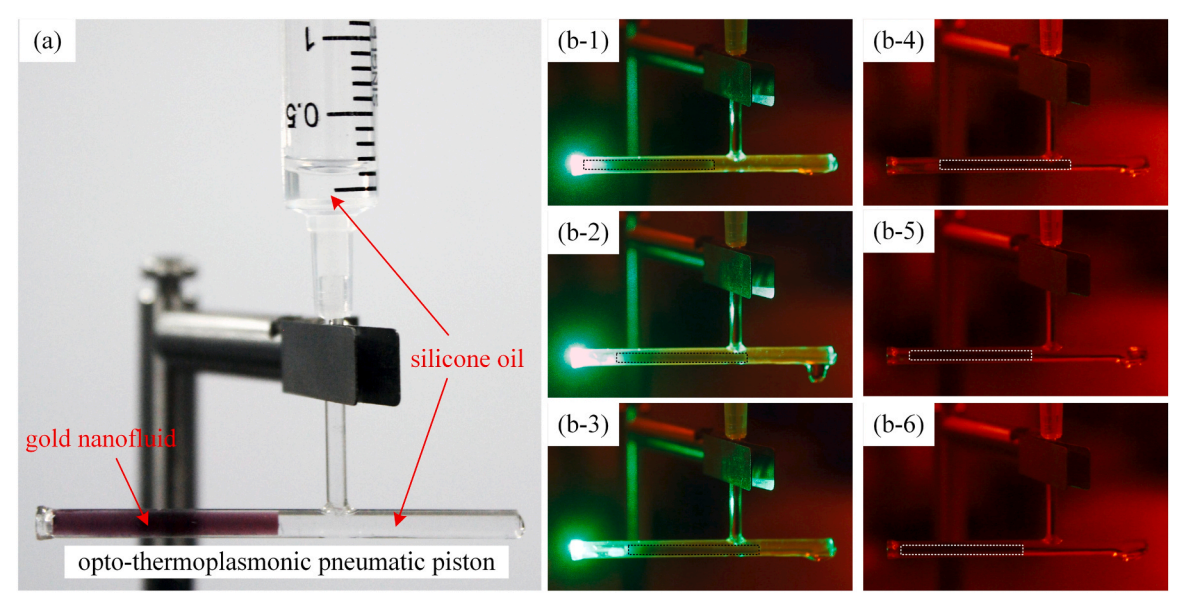


Fig. 10. The working cycle of opto-thermoplasmonic pneumatic piston pump. (a, The device of the pump; b, The working process of the opto-thermoplasmonic pneumatic piston pump).

concentration of nanofluids, the thermal conductivity of the casing, thermal diffusivity of the base liquid, and its vaporization latent heat. Increasing nanofluid concentration enhances thermal-to-kinetic energy conversion efficiency. For the cases in this study, the conversion efficiency of thermal energy to kinetic energy is only about $10^{-10}.$ And the output power is 6.8×10^{-7} mW. Most thermal energy escapes through the tube walls instead of converting into the liquid column's kinetic energy. Preventing heat loss through the tube walls can significantly improve the conversion efficiency of thermal energy to kinetic energy.

Due to limitations in laser spot size and processing methods, this study only experimentally investigated the performance of actuators with a 1.8 mm inner diameter. Combined with previous experimental results[12], reducing the inner diameter of the actuator can achieve a larger amplitude of piston movement and higher operating frequencies, greatly enhancing the performance of the actuator. The actuator can be utilized as a signal converter in mechanical and control fields. For example, in this study it converts the square wave signal of laser switching into a sawtooth wave signal of liquid piston movement.

In addition to functioning as a signal converter, the actuator can also serve as a controller and a driver. Although the actuator's output power is low, this provides a potential direction for its application. The device in Fig. 10a is modified from the opto-thermoplasmonic pneumatic pistons actuator, serving as a microfluidic plunger pump and fluid valve. The nanofluid in the T-shaped tube serves as both the power source and the plunger, with the branch pipe connecting an oil reservoir to supply silicone oil to the main pipe. Fig. 10b shows one working cycle of the actuator, and the operation process is detailed in the Movie S3 of supplementary video. When the laser irradiates the left end of the nanofluid piston, steam is generated, pushing a certain volume of silicone oil out of the device, while the nanofluid liquid column blocks the branch pipe, preventing the silicone oil in the reservoir from flowing downward. When the laser irradiation stops, the steam in the tube condenses, and the nanofluid piston returns to its initial position, opening the branch pipe and allowing the silicone oil in the reservoir to flow into the main pipe. This cycle repeats, continuously pumping silicone oil outward. By controlling the laser irradiation time, the volume of silicone oil pumped by the nanofluid liquid column can be precisely adjusted, showing promising applications in microfluidics and chemical engineering.

Supplementary material related to this article can be found online at doi:10.1016/j.sna.2025.116515.

4. Conclusions

By innovatively managing plasmonic heating, liquid evaporation, and condensation in opto-thermoplasmonic fluidics, we propose a new method to drive liquid piston movement by vapor pressure arising from photo-induced asymmetric evaporation, which relies on neither wetting gradients nor the Marangoni effect. The liquid piston can move rapidly, and its cyclic oscillation can be facilely regulated by adjusting the laser sources. The actuator characteristics have been investigated in detail. The oscillatory motion behavior is analogous to a pneumatic piston that can be described by a Kelvin-Voigt model with elastic and viscous components. The piston is able to work in phase with the excitation laser beam in the range of 0.05-3.6 Hz, and we believe that a more sensitive oscillation movement at high frequencies could also be expected if smaller tube sizes are used. The oscillating amplitude exhibits an exponential decay with the working frequency $l_a = a(1 - e^{-f_a^{-1}/b})$. Based on the theoretical analysis and experimental data, it is found that coefficient a is related to the laser power, piston length, and nanofluid concentration, while coefficient b is only dependent on the nanofluid concentration. This novel actuator consolidates the moving and power conversion components into one, simplifying the actuator's structure. It can work not only with simple liquids but also with complex fluids, creating new opportunities in the development of soft robots for biomedical, chemical, and other applications.

CRediT authorship contribution statement

Liu Guohua: Writing – review & editing. **Zhang Yuqian:** Investigation, Formal analysis. **Yan Xin:** Writing – original draft, Supervision, Project administration, Funding acquisition. **Wang Hongbiao:** Investigation, Data curation. **Xu Jinliang:** Writing – review & editing, Supervision.

Declaration of Competing Interest

The authors declare that they have no known competing financial interests or personal relationships that could have appeared to influence the work reported in this paper.

Acknowledgements

The research was supported by the National Natural Science Foundation of China (52306195) and the Fundamental Research Funds for the Central Universities (2023MS026).

Appendix A. Supporting information

Supplementary data associated with this article can be found in the online version at doi:10.1016/j.sna.2025.116515.

Data Availability

Data will be made available on request.

References

- [1] A. Garcia, J. Cusido, J.A. Rosero, J.A. Ortega, L. Romeral, Reliable electromechanical actuators in aircraft, Ieee Aerosp. Electron. Syst. Mag. 23 (2008), 19-+.
- [2] C.T. Nguyen, H. Phung, T.D. Nguyen, C. Lee, U. Kim, D. Lee, et al., A small biomimetic quadruped robot driven by multistacked dielectric elastomer actuators, Smart Mater. Struct. 23 (2014) 065005.
- [3] G.P. Kanakaris, N. Fatsis-Kavalopoulos, L.G. Alexopoulos, Laser activated singleuse micropumps, Sens. Actuators B: Chem. 220 (2015) 549–556.
- [4] K. Okano, A. Nogami, K. Asakura, High-strength gel actuator driven by a photothermal effect, Polym. J. 46 (2014) 827–830.
- [5] R. Tang, W. Sang, Y. Wu, C. Zhu, J. Liu, Multi-wavelength light drivable oscillatory actuator on graphene-based bilayer film, Macromol. Mater. Eng. 302 (2017) 1600384.
- [6] J.A. Lv, Y. Liu, J. Wei, E. Chen, L. Qin, Y. Yu, Photocontrol of fluid slugs in liquid crystal polymer microactuators, Nature 537 (2016) 179–184.
- [7] F. Terao, M. Morimoto, M. Irie, Light-driven molecular-crystal actuators: rapid and reversible bending of rodlike mixed crystals of diarylethene derivatives, Angew. Chem. Int Ed. Engl. 51 (2012) 901–904.
- [8] Y. Takashima, S. Hatanaka, M. Otsubo, M. Nakahata, T. Kakuta, A. Hashidzume, et al., Expansion-contraction of photoresponsive artificial muscle regulated by hostguest interactions, Nat. Commun. 3 (2012) 1270.
- [9] P. Yuan, J.M. McCracken, D.E. Gross, P.V. Braun, J.S. Moore, R.G. Nuzzo, A programmable soft chemo-mechanical actuator exploiting a catalyzed photochemical water-oxidation reaction, Soft Matter 13 (2017) 7312–7317.
- [10] Y. Chen, J. Yang, X. Zhang, Y. Feng, H. Zeng, L. Wang, et al., Light-driven bimorph soft actuators: design, fabrication, and properties, Mater. Horiz. 8 (2021) 728–757.
- [11] P. Zhou, L. Chen, L. Yao, M. Weng, W. Zhang, Humidity- and light-driven actuators based on carbon nanotube-coated paper and polymer composite, Nanoscale 10 (2018) 8422–8427.
- [12] J.R. Velez-Cordero, M.G. Perez Zuniga, J. Hernandez-Cordero, An optopneumatic piston for microfluidics, Lab Chip 15 (2015) 1335–1342.
- [13] F. Meng, W. Hao, S. Yu, R. Feng, Y. Liu, F. Yu, et al., Vapor-Enabled Propulsion for Plasmonic Photothermal Motor at the Liquid/Air Interface, J. Am. Chem. Soc. 139 (2017) 12362–12365.
- [14] S. Petitgrand, B. Courbet, A. Bosseboeuf, Characterization of static and dynamic optical actuation of Al microbeams by microscopic interferometry techniques, J. Micromech. Microeng. 13 (2012) S113.
- [15] F.R. Szabo, P.E. Kladitis, Design, Modeling and Testing of Polysilicon Optothermal Actuators for Power Scavenging Wireless Microrobots, Int. Conf. Mems (2004).

- [16] E. Wang, M.S. Desai, S.W. Lee, Light-controlled graphene-elastin composite hydrogel actuators, Nano Lett. 13 (2013) 2826–2830.
- [17] Z. Wang, X. Quan, W. Yao, L. Wang, P. Cheng, Plasma resonance effects on bubble nucleation in flow boiling of a nanofluid irradiated by a pulsed laser beam, Int. Commun. Heat. Mass Transf. 72 (2016) 90–94.
- [18] R. Saidur, K.Y. Leong, H.A. Mohammad, A review on applications and challenges of nanofluids, Renew. Sustain. Energy Rev. 15 (2011) 1646–1668.
- [19] N.J. Halas, S. Lal, S. Link, W.S. Chang, D. Natelson, J.H. Hafner, et al., A plethora of plasmonics from the laboratory for nanophotonics at Rice University, Adv. Mater. 24 (2012) 4842–4877, 774.
- [20] H. Šípová-Jungová, D. Andrén, S. Jones, M. Käll, Nanoscale Inorganic Motors Driven by Light: Principles, Realizations, and Opportunities, Chem. Rev. 120 (2020) 269–287.
- [21] U.G. Bütaitė, G.M. Gibson, Y.-L.D. Ho, M. Taverne, J.M. Taylor, D.B. Phillips, Indirect optical trapping using light driven micro-rotors for reconfigurable hydrodynamic manipulation, Nat. Commun. 10 (2019) 1215.
- [22] Y. Liu, Y. Zhang, C. Wang, Y. Wang, K. Zhang, X. Yang, et al., Multiplexed optofluidic laser immunosensor for sensitive and rapid detection of biomarkers, Sens. Actuators B: Chem. 403 (2024) 135198.
- [23] D. Baigl, Photo-actuation of liquids for light-driven microfluidics: state of the art and perspectives, Lab Chip 12 (2012) 3637–3653.
- [24] C. Gao, L. Wang, Y. Lin, J. Li, Y. Liu, X. Li, et al., Droplets Manipulated on Photothermal Organogel Surfaces, Adv. Funct. Mater. 28 (2018) 1803072.
- [25] H. Kawashima, A. Shioi, R.J. Archer, S.J. Ebbens, Y. Nakamura, S. Fujii, Light-driven locomotion of a centimeter-sized object at the air-water interface: effect of fluid resistance, RSC Adv. 9 (2019) 8333–8339.
- [26] M. Ito, H. Mayama, Y. Asaumi, Y. Nakamura, S. Fujii, Light-Driven Locomotion of Bubbles, Langmuir 36 (2020) 7021–7031.
- [27] L. Jauffred, A. Samadi, H. Klingberg, P.M. Bendix, L.B. Oddershede, Plasmonic Heating of Nanostructures, Chem. Rev. 119 (2019) 8087–8130.
- [28] X. Yan, J. Xu, Z. Meng, J. Xie, H. Wang, A New Mechanism of Light-Induced Bubble Growth to Propel Microbubble Piston Engine, Small 16 (2020) 2001548.
- [29] H. Jin, G. Lin, L. Bai, A. Zeiny, D. Wen, Steam generation in a nanoparticle-based solar receiver, Nano Energy 28 (2016) 397–406.
- [30] A. Terray, J. Oakey, D.W. Marr, Microfluidic control using colloidal devices, Science 296 (2002) 1841–1844.
- [31] B.R. Munson, T.H. Okiishi, W.W. Huebsch, A.P. Rothmayer, Fluid mechanics, Wiley. Singapore, 2013.
- [32] R.M. Christensen, Chapter I Viscoelastic Stress Strain Constitutive Relations, in: R. M. Christensen (Ed.), Theory of Viscoelasticity (Second Edition), Academic Press, 1982, pp. 1–34.

Hongbiao Wang studies in North China Electric Power University as a Master's student, and his research interests focus on the optofluidics.

Jinliang Xu is a professor in North China Electric Power University. His interests focus on the microfluidics and their applications.

Yuqian Zhang studies in North China Electric Power University as a Master's student, and his research interests focus on the plasma effect of nanofluid.

Xin Yan is an assistant researcher in North China Electric Power University. His interests focus on the optofluidics and their applications.

Guohua Liu a professor in North China Electric Power University. His interests focus on the design and fabricate of novel micro-device on energy conversion.